Mesoporous silica nanoparticle-based protein delivery systems for biomedical applications

Tu, J.

Chapter II

Mesoporous Silica Nanoparticles with Large Pores for the Encapsulation and Release of Proteins

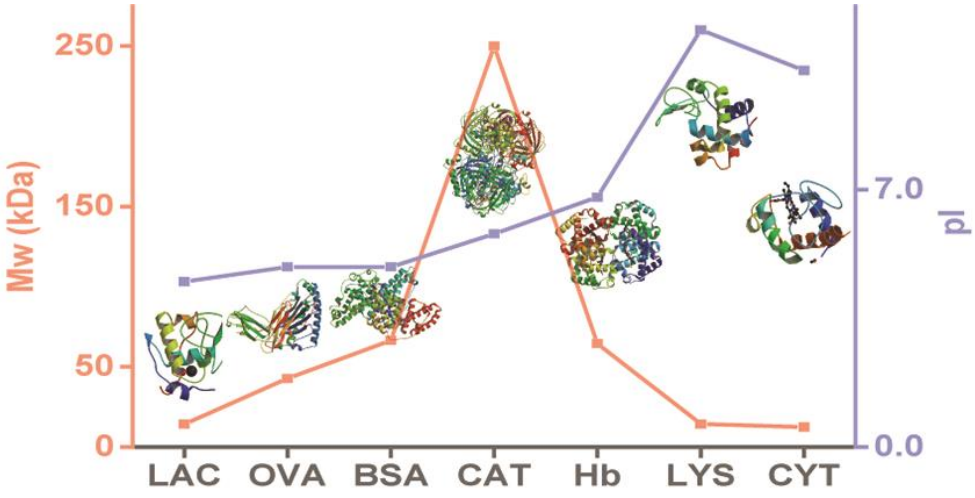

Jing Tu, Aimee L. Boyle, Heiner Friedrich, Paul H.H. Bomans, Jeroen Bussmann, Nico A.J.M. Sommerdijk, Wim Jiskoot, and Alexander Kros, *ACS Appl. Mater. Interfaces,* **2016**, DOI: 10.1021/acsami.6b11324

Abstract

Mesoporous silica nanoparticles (MSNs) have been explored extensively as solid supports for proteins in biological and medical applications. Small (< 200 nm) MSNs with ordered large pores (> 5 nm), capable of encapsulating therapeutic small molecules suitable for delivery applications *in vivo*, are rare however. Here we present small, elongated, cuboidal, MSNs with average dimensions of 90 × 43 nm that possess disk-shaped cavities, stacked on top of each other, which run parallel to the short axis of the particle. Amine-functionalization was achieved by modifying the MSN surface with 3-aminopropyltriethoxysilane or 3-[2-(2-aminoethylamino)ethylamino] propyltrimethoxysilane (AP-MSNs and AEP-MSNs) and were shown to have similar dimensions to the non-functionalized MSNs. The dimensions of these particles, and their large surface areas as measured by nitrogen adsorption-desorption isotherms, make them ideal scaffolds for protein encapsulation and delivery. We therefore investigated the encapsulation and release behavior for seven model proteins (α-lactalbumin, ovalbumin, bovine serum albumin, catalase, hemoglobin, lysozyme and cytochrome c). It was discovered that all types of MSNs used in this study allow rapid encapsulation, with a high loading capacity, for all proteins studied. Furthermore, the release profiles of the proteins were tunable. The variation in both rate and amount of protein uptake and release was found to be determined by the surface chemistry of the MSNs, together with the isoelectric point (pI), and molecular weight of the proteins, as well as by the ionic strength of the buffer. These MSNs with their large surface area and optimal dimensions, provide a scaffold with a high encapsulation efficiency and controllable release profiles for a variety of proteins, enabling potential applications in fields such as drug delivery and protein therapy.

Keywords: mesoporous silica nanoparticles, protein loading, protein release, nanomedicine, sol-gel, drug delivery

2.1 Introduction

Proteins participate in a variety of vital processes in the body,[1] and are therefore used as therapeutic agents in a diverse range of biomedical applications,[2] such as cancer therapy,[3, 4] vaccination,[5, 6] and protein therapy.[7, 8] Several barriers have to be overcome for efficient protein delivery however, as most native proteins are membrane impermeable due to electrostatic repulsion, and are prone to degradation or inactivation processes in bodily fluids.[1] Over the last decades, various nanocarriers such as lipid-based assemblies,[9] gold nanoparticles[10] and polymeric nanoparticles,[11] have been developed to overcome these barriers.

Mesoporous silica nanoparticles (MSNs) are a class of molecules that have attracted a lot of attention in the small molecule delivery field, due to their multitude of desirable properties. They possess an open-pore structure; the sizes of the pores and of the MSNs themselves can be controlled synthetically.[12-14] Furthermore, the silanol-containing surface can be readily functionalized,[15-17] enabling modification with targeting molecules such as folate or hyaluronic acid to enhance cellular uptake,[18, 19] and permitting the adsorption of various proteins with different isoelectric points (pI).[16, 20] Due to their structure, MSNs protect proteins from premature degradation in body fluids, thereby increasing the efficiency of protein delivery *in vivo*, thus reducing renal filtration.[1] This combination of properties means MSNs have exhibited potential as a non-invasive and biocompatible platform for protein delivery,[21, 22] especially in the fields of enzyme therapies,[7, 8] vaccination,[5, 6, 23] and imaging.[24] Since MSNs are much smaller than eukaryotic cells, they can facilitate the transport of proteins into the cytosol via an endocytosis pathway and subsequent endosomal escape.[25, 26]

Numerous synthetic protocols for the preparation of MSNs have been developed with the aim of controlling the size and morphology of these nanoparticles.[27-30] Encapsulating proteins in MSNs is still challenging however, and only a few publications concerning the design of MSNs with a morphology that enables the effective encapsulation of a broad range of proteins are available.[31, 32] Typically, proteins are only adsorbed onto the external surface of MSNs due to the small pore diameter (< 3 nm) preventing the proteins from entering the MSNs' interior pores.[5, 33] Proteins adsorbed at the MSNs' outer surface do not make use of the protective environment inside the MSNs, nor do they utilize the large internal surface area presented by the pores.[14, 34] Thus, limitations in generating small (< 200 nm in diameter) MSNs with sufficient pore sizes (> 5 nm) to encapsulate proteins or other biomacromolecules is one of the major hurdles for "comfortably" hosting large molecules.[21, 35-37] In order to solve

this protein inaccessibility issue, MSNs with a large pore size have been synthesized. However, the diameter of the majority of these particles is 1-2 μm and so these are less suited for *in vivo* delivery applications. Studies have shown that particle sizes between 50 and 200 nm are preferred for endocytic uptake.[25, 38, 39] Therefore, monodisperse MSNs with a particle size in the 50-200 nm range, controllable surface chemistry, and a large pore size (> 5 nm) are desired. [31, 36]

Building upon previous methods,[28, 40-42] we designed a facile synthetic route to produce MSNs that are able to effectively encapsulate and release a variety of proteins. To obtain the desired large pores in a sub-200 nm particle, a double-surfactant system consisting of a high molecular weight block copolymer (Pluronic P123),[28, 31, 40] and fluorocarbons,[28, 43] was employed as the structure-directing template. The swelling agent 1,3,5-trimethylbenzene (TMB) was added to expand the diameter of the pores.[28, 40] These MSNs were synthesized as stable colloidal suspensions with a narrow size distribution and channels aligned parallel to the short axis. This mesostructure favors efficient mass transfer,[44] as it possesses a high density of entrances enabling rapid and efficient encapsulation of proteins.[35]

The obtained MSNs bear a net negative charge,[29, 34] at physiological pH. To study the effect of the silica surface charge on protein encapsulation, cationic MSNs were prepared by a post-synthesis grafting method involving the amine-containing silanes (3-aminopropyl)triethoxysilane (APTES) and 3-[2-(2-aminoethylamino)ethylamino] propyltrimethoxysilane (AEPTMS). This modification generated positively charged MSNs at physiological pH, designated as AP-MSNs and AEP-MSNs, respectively.

To illustrate the potential of these new, large-pore MSNs as protein carriers, the encapsulation and release of a range of model proteins[20, 45-48] with different molecular weights (Mw) and isoelectric points (pI) was studied, revealing that the MSNs' surface charge controls the protein encapsulation efficiency. The release profiles of the proteins from these large-pore MSNs were subsequently examined, and it was additionally confirmed that the structure of the released proteins was not altered.

2.2 Materials and Methods

2.2.1 Materials

Pluronic P123 ($EO_{20}PO_{70}EO_{20}$, M_n~5800 g/mol), tetraethyl orthosilicate (TEOS, ≥98%), hydrochloric acid (HCl), mesitylene, 3-aminopropyltriethoxysilane (APTES), 3-[2-(2-aminoethylamino)ethylamino] propyltrimethoxysilane (AEPTMS), 1,3,5-trimethylbenzene

(TMB), α-lactalbumin from bovine milk (LAC), albumin from chicken egg white (OVA), bovine serum albumin (BSA), catalase from bovine liver (CAT), hemoglobin from bovine blood (Hb), cytochrome c from equine heart (CYT) and lysozyme from chicken egg white (LYS) were purchased from Sigma-Aldrich and used as received. Fluorocarbon surfactant FC-4 was purchased from Yick-Vic Chemicals & Pharmaceuticals (HK) Ltd, China. Milli-Q water (18.2 MΩ/cm, Millipore Co., USA) was used throughout the experiments. The composition of the phosphate buffered saline (PBS) used was: K_2HPO_4 (14.99 mM), KH_2PO_4 (5 mM), and NaCl (150.07 mM), with an ionic strength of 270 mM. The phosphate buffer (PB) with an ionic strength of 12 mM was prepared by mixing Na_2HPO_4 (1 mM) and NaH_2PO_4 (1 mM) at molar ratio of 5:2. The PB with an ionic strength of 166 mM was prepared by adding 0.9% NaCl into previously described PB with an ionic strength of 12 mM. The pH values were adjusted to 7.4.

2.2.2 Preparation of large-pore MSNs and functionalized MSNs

MSNs were synthesized as follows. 0.5 g of surfactant Pluronic P123 and 1.4 g of FC-4 were dissolved in 80 mL of HCl (0.02 M), followed by the introduction of 0.48 mL of TMB. After stirring for 6 h, 2.14 mL of TEOS was added dropwise. The resulting mixture was stirred at 30 °C for 24 h and transferred to an autoclave at 120 °C for 2 days. Finally, the solid product was isolated by centrifugation, and washed with ethanol and water. The organic template was completely removed by calcination at 550 °C for 5 h.

The MSNs were functionalized with amine-containing groups through a post-modification procedure.[49, 50] For AP-MSNs, 100 mg of MSNs were suspended in 10 mL of ethanol and 0.4 mL of APTES was added. The mixture was refluxed at 77 °C for 10 h with stirring. The resulting particles were collected by centrifugation (13000 rpm, 5 min), washed thoroughly with ethanol and water three times, and freeze-dried. For AEP-MSNs, 100 mg of MSNs were incubated with 4 mL of 20 wt% AEPTMS in ethanol, overnight at room temperature. The AEP-MSNs were purified by centrifugation (13000 rpm, 5 min) and washed with ethanol and water three times to remove unreacted AEPTMS, and freeze-dried.

2.2.3 Protein encapsulation studies

A protein stock solution (0.5 mg/mL) was prepared in phosphate buffer (1 mM, pH 7.4). MSNs, AP-MSNs, and AEP-MSNs (2 mg/mL), were sonicated (10 min) and dispersed in the same buffer. In a typical procedure, 0.5 mL of protein stock solution was mixed with 0.5 mL of MSNs, AP-MSNs or AEP-MSNs suspension and incubated in an Eppendorf mixer (400

rpm, 25 °C). After incubation for 20 min, protein-loaded particles (MSNs, AP-MSNs and AEP-MSNs) were collected by centrifugation (13000 rpm, 5 min) and separated from the non-encapsulated protein, which remained in the supernatant. The encapsulation efficiency (EE%) was determined by measuring the difference in concentration of the protein in the supernatant before and after loading. The concentration of protein was determined using a standard calibration curve of the corresponding protein. The intrinsic fluorescence intensity and absorbance of the proteins were measured using Greiner 96-well flat-bottom black, and Greiner 96-well flat-bottom transparent, microplates respectively in a plate reader (Tecan infinite M1000). For LAC, OVA, BSA, CAT and LYS, the standard curves were based on the intrinsic fluorescence intensity (excitation wavelength = 280 nm and emission wavelength = 320 nm) as a function of concentration (0-500 µg/mL). For Hb and CYT, the calibration curves were based on the absorbance at 405 nm and 412 nm respectively, as a function of concentration (0-500 µg/mL). The EE% and loading capacity (mg/g) were calculated as shown in Equation 2.1 and 2.2:[21, 51]

$$\text{EE\%} = \frac{t_{protein} - f_{protein}}{t_{protein}} \times 100\% \quad (2.1)$$

$$\text{Loading capacity (mg/g)} = \frac{t_{protein}(\text{mg}) - f_{protein}(\text{mg})}{\text{amount of MSNs (g)}} \quad (2.2)$$

Where $t_{protein}$ is the total amount of protein, and $f_{protein}$ is the amount of free protein.

2.2.4 Protein release studies

The *in vitro* release of encapsulated proteins, and the effect of ionic strength on the release profiles, was determined by suspending the protein-loaded MSNs in 1 mL of phosphate buffer of different ionic strengths (12 mM, 166 mM and 270 mM) at a final MSN concentration of 1 mg/mL. All suspensions were placed in an Eppendorf mixer (400 rpm, 37 °C). The amount of released protein was determined by removing the supernatant after centrifugation (13000 rpm, 5 min) and replacing it with clean buffer (1 mL) at specified time points. The amount of protein in the supernatant was measured using a Tecan infinite M1000 plate reader (using the settings described in section 2.3). All measurements were performed in triplicate. CD spectra of the proteins before and after release were measured using a Jasco J-815 spectropolarimeter. Spectra were collected from 260 – 190 nm, at 25 °C to determine whether encapsulation and subsequent release of the proteins had any effect on their secondary structure.

2.2.5 Particle analysis

The porous structure of the as-prepared MSNs was characterized using transmission electron microscopy (TEM) operated at 70 kV (TEM, JEOL 1010, USA). (Cryo-) electron tomography was performed in bright-field mode using zero-loss energy filtering with 20 eV energy window on the TU/e cryoTITAN (FEI, FEG, 300 kV, Gatan Energy filter). Images of the tilt-series were collected either dry at room temperature or under cryogenic conditions with the particles suspended in vitrified water over an angular range of ± 65° at 2 degree increments and with a nominal underfocus of -200 nm (dry) or -5 µm (cryo). Due to the beam sensitivity of the material, the total accumulated dose over the entire tilt-series was kept below 100 $e^-/Å^2$. Alignment by fiducial gold particles, 3D reconstruction and denoising using nonlinear anistropic diffusion was carried out in IMOD. Visualization was performed in Avizo. Surface analysis of the MSNs was performed by measuring nitrogen-sorption isotherms at 77 K with a Micromeritics TrisStar II 3020 as the analyzer. As a pretreatment, MSNs were outgassed at 300 °C for 16 h under vacuum (below 0.15 mbar), while the other samples (AP-MSNs, AEP-MSNs, and protein-loaded MSNs) were outgassed at 25 °C for 16 h. The specific surface areas were calculated using the Brunauer-Emmett-Teller (BET) method. The pore size distribution was calculated from the desorption branch of the isotherm by the Barrett-Joyner-Halenda (BJH) method.[52] The hydrodynamic diameter and zeta-potential of the MSNs were measured with a Malvern Nano-ZS instrument.

2.3 Results and discussion

2.3.1 Synthesis and characterization of MSNs, AP- and AEP-MSNs

Existing literature details how amphiphilic block copolymers such as Pluronic P123,[31, 40] act as organic structure-directing agents, and co-solvent organic molecules (*e.g.* TMB)[53, 54] can be used as swelling agents to obtain MSNs with large pores. This technique was replicated here and, in addition, the cationic fluorocarbon surfactant FC-4 was utilized to confine the diameter of the MSNs.[28] Additionally, a hydrothermal treatment, similar to the procedure reported by Han,[28, 55] but with a higher temperature (120 °C) and a longer reaction time (48 h) was employed to improve mesoscopic regularity and to further extend pore size.[40, 42, 56, 57]

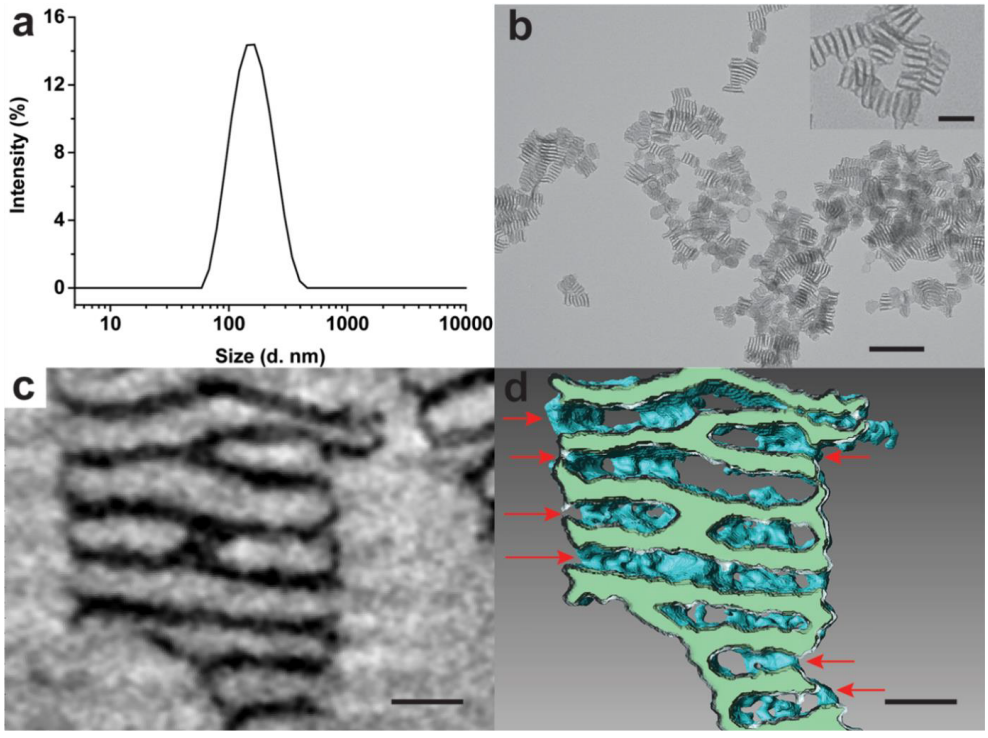

Figure 2.1 *(a) Hydrodynamic diameter by DLS; (b) TEM image of MSNs, scale bar = 200 nm, insert figure with scale bar = 50 nm, (c) and (d) electron tomography results showing cross-section through reconstruction (pores that connect cavities with the environment are indicated by arrows) and 3D rendering of silica surface (cut to expose the interior), scale bar = 25 nm.*

Dynamic light scattering (DLS) measurements revealed MSNs with a unimodal distribution that possessed an average hydrodynamic diameter of 146 nm (Figure 2.1a). The morphology and mesoporous structure of the MSNs was visualized by TEM (Figure 2.1b). Analysis of the TEM images revealed the MSNs had lengths of 90 ± 20 nm and widths of 43 ± 7 nm, giving them an elongated cuboidal-like geometry. These sizes were slightly smaller than those determined by DLS, since TEM provides the size distribution of dehydrated particles and DLS measurements yield an average hydrodynamic diameter of the particles in solution.[58] The MSNs were found to possess large channels with an average size of 10 ± 1 nm (measurements from 150 particles). These channels run parallel to the short axis of the MSNs.

Next, a 3D-reconstruction of the MSNs was obtained by (cryo-) electron tomography. This revealed the MSNs possessed disk-shaped cavities, or channels, stacked on top of each

other, which run parallel to the short axis of the particle, consistent with the TEM observations (Figure 2.1c,d).

To further characterize the channels within the MSNs, nitrogen sorption measurements were performed. The MSNs exhibit characteristic type IV isotherms with type-H_1 hysteresis loops[40, 59] in nitrogen sorption measurements, indicative of the presence of channel-like mesopores (Figure 2.2a). The average diameter of the channels inside these MSNs was calculated to be 9-11 nm (Figure 2.2b), consistent with the result obtained by TEM. The MSNs were calculated to have a large specific surface area of 506 m^2/g (Table 2.1).

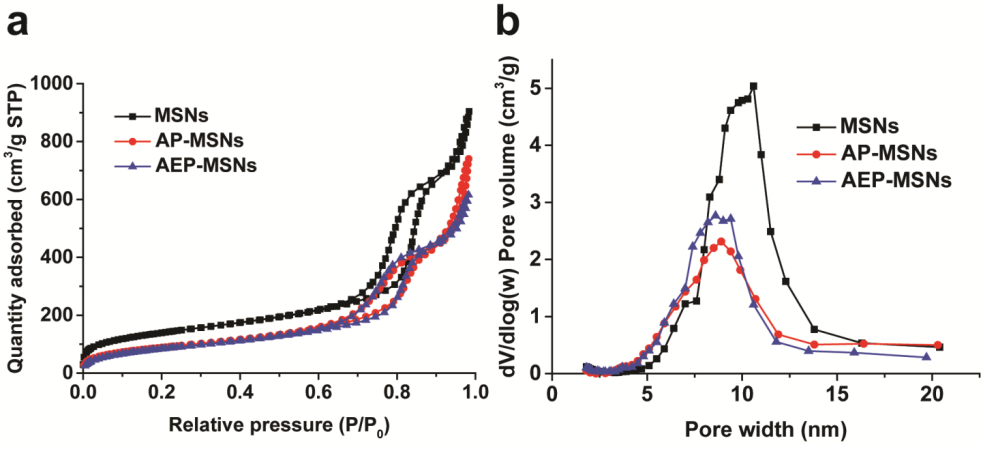

Figure 2.2 *(a) Nitrogen adsorption-desorption isotherms and; (b) corresponding pore size distributions of MSNs, AP-MSNs and AEP-MSNs.*

Amino-modified MSNs, termed AP- and AEP-MSNs, were synthesized by reacting the MSNs with APTES, and AEPTMS respectively. These modified MSNs also exhibited type IV isotherms with type-H_1 hysteresis loops (Figure 2.2a), indicating functionalization of the surface of the MSNs with amine groups did not perturb the structure. The presence of amino groups does reduce the specific surface area to 328 m^2/g and 318 m^2/g for AP-MSNs and AEP-MSNs respectively (Table 2.1). This is in accordance with the slightly reduced pore diameters of AP- and AEP-MSNs, which are both calculated to be 9 ± 1 nm (Figure 2.2b,Table 2.1), which is still larger than the geometric size of most proteins.

Table 2.1 Physical characteristics of MSNs, AP-MSNs and AEP-MSNs

Sample	BET specific surface area (m^2/g)	Specific channel volume (cm^3/g)	Average channel diameter (nm)[a]
MSNs	506	1.01	10 ± 1
AP-MSNs	328	0.68	9 ± 1
AEP-MSNs	318	0.71	9 ± 1

[a]*Calculated from the desorption branch of the N_2 sorption isotherms based on the BJH method.*

2.3.2 Protein loading studies

To test the potential of these MSNs for protein-based delivery applications we studied the encapsulation and release of seven model proteins with different molecular weights, geometric sizes, shapes, and pI values (Table 2.2). These proteins were selected due to the wide variety of physical properties they collectively presented, (Table 2.2), and because of their biological applications, for example: ovalbumin has been studied for its antigenic properties;[5, 6] catalase is an important antioxidant;[7, 8] hemoglobin is a well-characterised oxygen carrier;[51, 60] and cytochrome c has been known to induce apoptosis.[53, 61]

Table 2.2 List of encapsulated proteins and their properties

Protein	Classification[a]	Mw/kDa	Size[b] (nm)	pI
LAC	glycoprotein	14.2	2.3 × 2.6 × 4	4.5
OVA	allergen	42.7	4 × 5 × 7	4.9
BSA	transport protein	66.5	5 × 5 × 9	4.9
CAT	oxidoreductase	250	7 × 8 × 10	5.8
Hb	oxygen binding	64.5	5.3 × 5.4 × 6.5	6.8
LYS	hydrolase	14.3	3 × 3 × 4.5	10-10.5
CYT	electron transport	12.4	2.6 × 3.2 × 3.3	11.35

[a]*The classification and residue count of these proteins comes from the protein data bank (PDB, www.rcsb.org). PDB codes: LAC, 1HFX; OVA, 1VAC; BSA, 4F5S; CAT, 1TGU; Hb, 2QSS; LYS, 4YM8; CYT, 2N3B.*

[b]*Geometric dimensions given by published literature.*[34, 62-64]

Proteins were mixed with MSNs, AP- and AEP-MSNs in a 1:4 (protein:MSN) weight ratio. Figure 2.3a shows the encapsulation efficiency (EE%) of these proteins at physiological pH. The encapsulation process was found to be very rapid, with over 95% encapsulation efficiency being achieved within twenty minutes for all proteins.

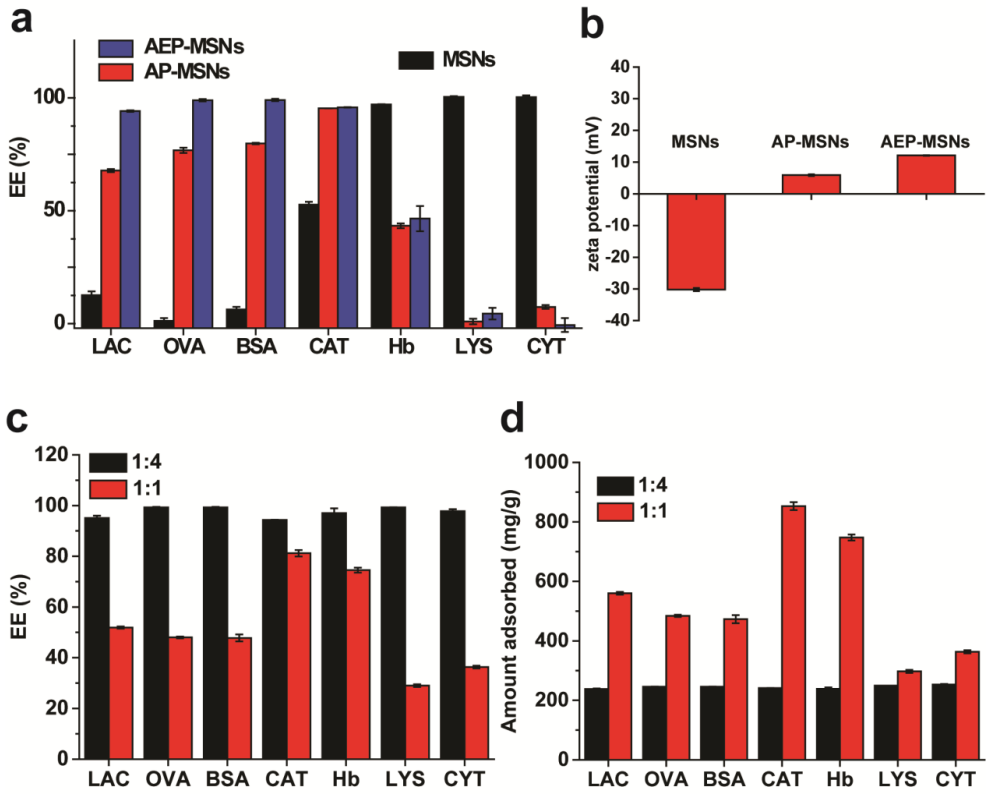

Figure 2.3 *(a) EE% of seven proteins in MSNs (black bars), AP-MSNs (red bars), and AEP-MSNs (blue bars), the initial weight ratio for encapsulation between protein and particles was 1:4 (250 mg of protein/1 g particles); (b) zeta potential of MSNs, AP-MSNs and AEP-MSNs in 1 mM PB, pH 7.4; (c) Encapsulation efficiency (EE%) of seven proteins (LAC, OVA, BSA and CAT in AEP-MSNs, and Hb, LYS and CYT in MSNs), and (d) the corresponding loading capacity (mg/g) for all proteins. The weight ratio for encapsulation between protein and MSNs is 1:4 (black bars) and 1:1 (red bars). Conditions for encapsulation of all proteins: 1 mM PB, ionic strength 12 mM, 25 °C, 20 min.*

The charges of the MSNs, AP-MSNs and AEP-MSNs vary due to the surface chemistry of the particles. Zeta-potential analysis (Figure 2.3b), revealed a negative surface charge for MSNs (-30.2 mV), but a positive charge for both AP- and AEP-MSNs (+5.9 mV and +12.1 mV, respectively). This charge affects the extent of protein encapsulation; for proteins with a negative surface charge (LAC, OVA, BSA and CAT), encapsulation in positively charged AP- and AEP-MSNs was more efficient when compared to encapsulation in unmodified

MSNs. This was especially relevant with AEP-MSNs, where the encapsulation efficiency for all four of these proteins reached more than 95%. It is therefore evident that the amount of LAC, OVA, BSA and CAT encapsulated can be increased by the introduction of positively charged amine moieties onto the MSNs surface. Conversely, for the positively charged proteins LYS and CYT the amount encapsulated decreases when AP- or AEP-MSNs are employed. The observed results indicate that electrostatic interactions are likely to be the main driving force for protein encapsulation.[45, 65, 66] It is also interesting to note that CAT (250 kDa, *ca.* 10 nm diameter)[46] can be encapsulated into the mesopore network despite the fact that the pore size is similar to that of protein.[67] Interestingly, Hb (pI = 6.8) is still negatively charged when dissolved in phosphate buffer at pH 7.4. Still, the EE% of Hb reached 97%, while for AP-MSNs the EE% was 43% and for AEP-MSNs, 47%. For positively charged proteins (LYS and CYT), a high encapsulation efficiency (97% and 98% respectively), was obtained with unmodified MSNs while the encapsulation in AP-MSNs and AEP-MSNs was limited due to electrostatic repulsion.

Considering the initial weight ratio between the proteins and MSNs (1:4), and the EE%, these results clearly showed that MSNs (with an appropriate surface charge) can act as nanocarriers to efficiently encapsulate a wide variety of proteins (Mw 12.3-250 kDa, pI 4.5-11.3) with a loading capacity of at least 25 wt% (250 mg/g). When the initial weight ratio between the proteins and MSNs was increased (1:1), the EE% decreased but the total amount of protein encapsulated increased. For example, the loading capacity of CAT into AEP-MSNs increased from 241.7 ± 0.4 mg/g to 852.9 ± 13.2 mg/g, while for Hb 239.1 ± 4.6 mg/g was encapsulated at the 1:4 ratio, but this rose to 747.5 ± 10.0 mg/g when a 1:1 ratio was used. For LAC an increase from 238.0 ± 2.3 mg/g to 560.0 ± 4.4 mg/g was observed (Figure 2.3c,d). The large pore size is advantageous, especially for proteins with a high molecular weight and hence a large size. Upon protein encapsulation, both the surface area and pore diameter of the MSNs decreased, showing that the protein molecules had been encapsulated within the channels of the MSNs (Figure 2.4 and Table 2.S1).[31]

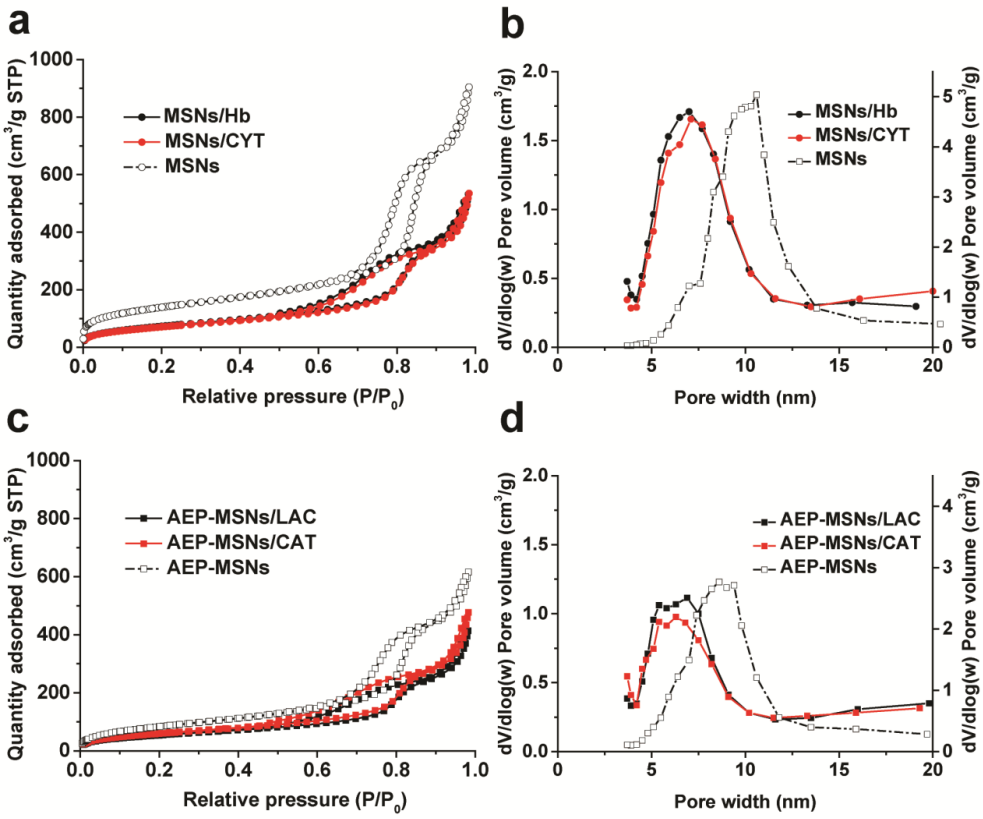

Figure 2.4 *(a) Nitrogen adsorption-desorption isotherms of MSNs/proteins (Hb and CYT), and (b) corresponding pore size distributions, with MSNs as a control; (c) nitrogen adsorption-desorption isotherms of AEP-MSNs/proteins (LAC and CAT), and corresponding (d) pore size distributions, with AEP-MSNs as a control.*

2.3.3 Protein release studies

The *in vitro* release of proteins from MSNs or AEP-MSNs was investigated using a high ionic strength (270 mM) PBS buffer. For this study MSNs containing Hb, LYS and CYT, and AEP-MSNs loaded with LAC, OVA, BSA and CAT were tested. All the profiles showed a rapid burst release (Figure 2.5),[68] and a direct correlation between the final released percentage and the molecular weight of the protein was observed.

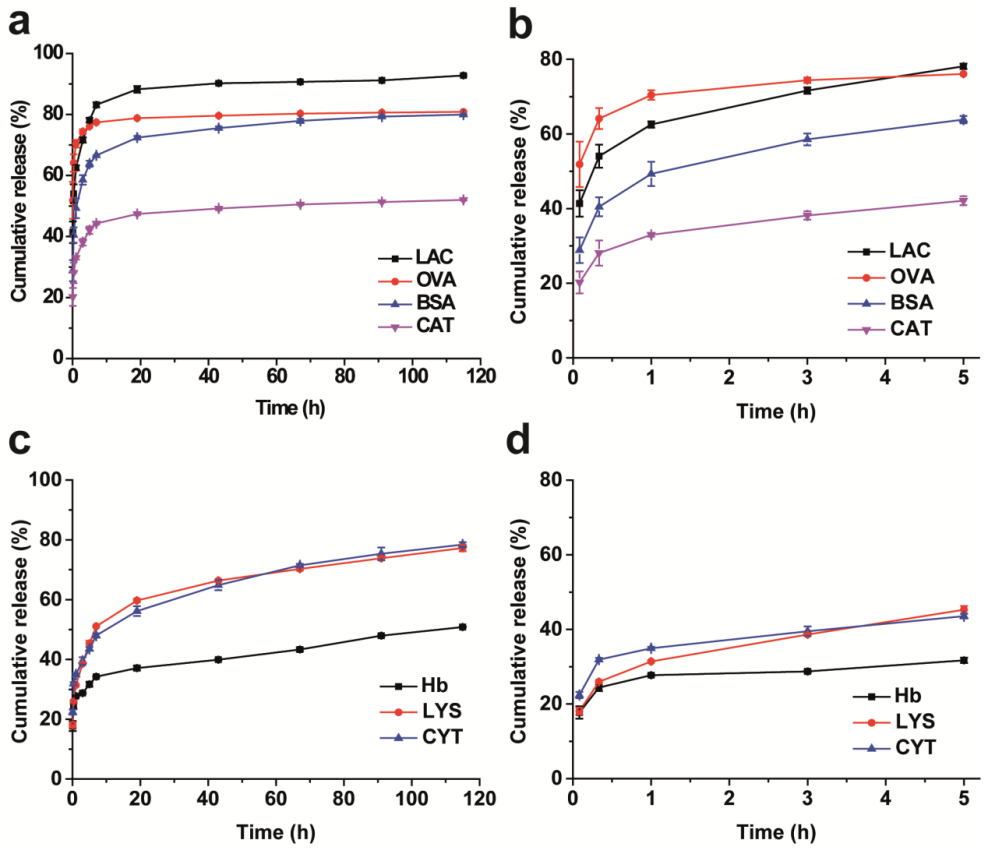

Figure 2.5 *(a) and (b) LAC, OVA, BSA and CAT release profiles from AEP-MSNs and; (c) and (d) Hb, LYS and CYT release profiles from MSNs. Conditions for release of all proteins: PBS, (ionic strength 270 mM), 37 °C.*

A large amount of the encapsulated LAC (93%) was released from AEP-MSNs. This was the smallest protein to be encapsulated into these MSNs, so it is rational that this shows the highest released percentage as its small size makes 'escape' from the pores easier. OVA and BSA showed comparable release percentages (81 and 80%, respectively). These proteins are similar in size, therefore it is unsurprising that the amounts released are similar. They are significantly larger than LAC however, and the high release percentages are encouraging as these reveal that reasonably large proteins can escape from the MSN channels. Only 52% of CAT, the largest protein to be encapsulated in the AEP-MSNs was released however. The dimensions of CAT are 7 × 8 × 10 nm, this is close to the diameter of the pores and so it is possible that this protein gets trapped inside the pores resulting in a lower released percentage.

For the proteins encapsulated in the unmodified MSNs, a similar trend was seen. The two smallest proteins, CYT and LYS, exhibited similar release percentages (78 and 77% respectively). For Hb, the largest protein encapsulated into these MSNs, only 41% was released over the time frame studied, indicating that size plays an important role in release dynamics in these MSNs as well.

The effect of the ionic strength of the buffer on the proteins' release kinetics was also investigated (Figure 2.S1). Comparison of Figure 2.5a,b with Figure 2.S1a,b clearly shows the effect of ionic strength on the AEP-MSNs encapsulated proteins' release. When a low ionic strength buffer was used, the amount of protein released decreased for all the proteins investigated. The largest decrease was seen for LAC; 93% of the encapsulated protein was released when PBS with an ionic strength of 270 mM was used, this decreased to 69% for 166 mM PB buffer and a further decrease to 21% was observed when PB buffer with 12 mM ionic strength was employed, with the other proteins following a similar trend. These results indicate that a higher ionic strength of the buffer and a smaller molecular weight of the protein results in a larger percentage of released protein. This is likely to be because a smaller protein can escape the channels more easily, and a higher ionic strength buffer,[16] screens electrostatic interactions more effectively, meaning the electrostatic interactions that are holding the proteins in place in the MSNs are diminished.

The release of the MSN-encapsulated proteins did not follow such a clear trend when the ionic strength of the buffer was changed; compare Figure 2.5c,d and 2.S1c,d. At low ionic strength, the initial release rate of LYS was very low; this increased with an increasing buffer strength, as did the total amount of protein released. Hb and CYT exhibited different properties however. Both proteins showed burst release kinetics at high ionic strengths, whereas at low ionic strength the release was more sustained. The total amount released did not change as much for these proteins upon altering the ionic strength of the buffer (24, 27%, and 51% for Hb and 54, 69%, and 78% for CYT at 12 mM, 166 mM, and 270 mM ionic strength respectively) as it did for others. This suggests the factors controlling the release from the negatively-charged MSNs are more subtle than from the AEP-MSNs. Both protein size and charge (distribution) have an effect, but the effects of these are not easily separated. It would be interesting for future work to study the release of more proteins with MSNs to disentangle these effects and to determine which is more important – molecular weight or charge of the protein.

Finally, for any application, it is important that the released proteins are not misfolded, for example, due to strong MSN-protein interactions. Therefore the secondary structure of the

released proteins was compared to that of non-encapsulated proteins. The structures were measured using circular dichroism (CD) spectroscopy and no change was seen in any of the protein's secondary structure after encapsulation and release (Figure 2.S2).

2.4 Conclusion

Here we have described a method to synthesize sub-200 nm MSNs with large (10 nm) channels perpendicular to the long axis of the particles. As a result, the MSNs (or the facilely modified AP- and AEP-MSNs) have a rapid, high encapsulation efficiency of a wide range of proteins with vastly different properties. Encapsulation was found to be dependent on the surface chemistry within the channels, and was directly related to the surface charge of the protein. The release of such proteins is tunable, and is dependent on the ionic strength of the release medium and the MSN surface chemistry. Protein properties such as molecular weight and charge also play a role in the release kinetics, with the parameters governing release being more subtle and involved than those controlling encapsulation.

This novel type of MSN with large channels and therefore a high surface area, resulting in a high encapsulation efficiency and controllable release profiles of proteins enables potential applications in fields such as protein therapy and drug delivery.

Supporting Information

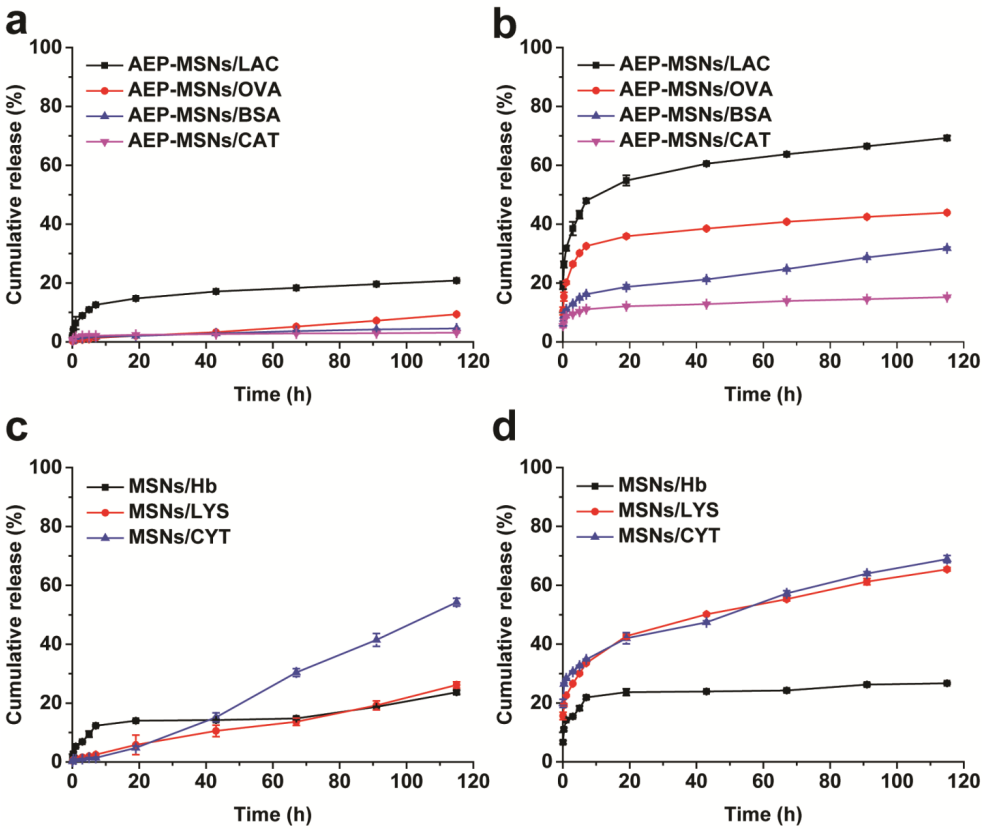

Figure 2.S1 *LAC, OVA, BSA and CAT release profiles from AEP-MSNs in (a) 1 mM PB (ionic strength 12 mM), and (b) 1 mM PB with 0.9% NaCl at 37 °C (ionic strength 166 mM); Hb, LYS and CYT release profiles from MSNs in (c) 1 mM PB (ionic strength 12 mM), and (d) 1 mM PB with 0.9% NaCl at 37 °C (ionic strength 166 mM).*

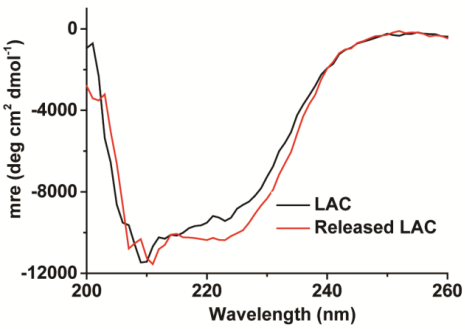
mre (deg cm^2 dmol^{-1})
0
-4000
-8000
-12000
200
220
240
260
Wavelength (nm)
LAC
Released LAC

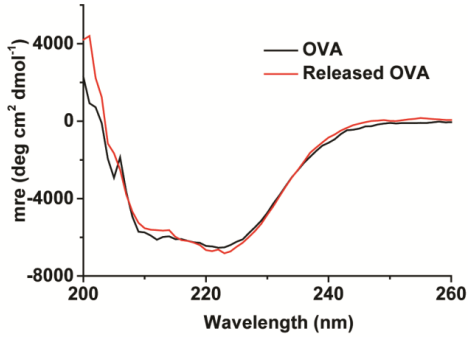
mre (deg cm^2 dmol^{-1})
4000
0
-4000
-8000
200
220
240
260
Wavelength (nm)
OVA
Released OVA

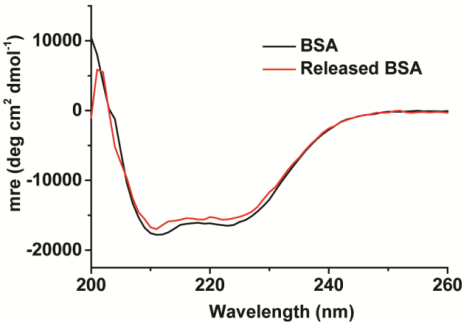
mre (deg cm^2 dmol^{-1})
10000
0
-10000
-20000
200
220
240
260
Wavelength (nm)
BSA
Released BSA

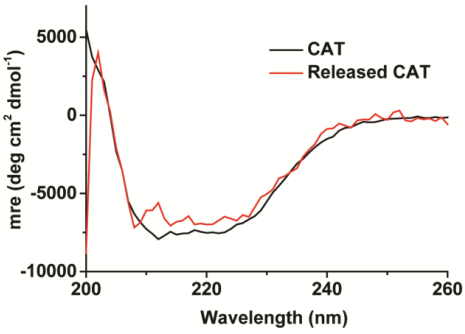
mre (deg cm^2 dmol^{-1})
5000
0
-5000
-10000
200
220
240
260
Wavelength (nm)
CAT
Released CAT

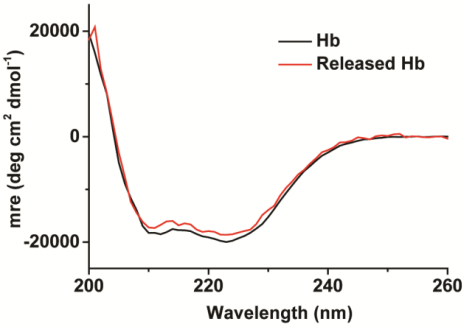
mre (deg cm^2 dmol^{-1})
20000
0
-20000
200
220
240
260
Wavelength (nm)
Hb
Released Hb

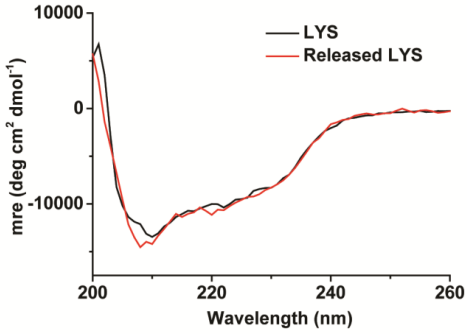
mre (deg cm^2 dmol^{-1})
10000
0
-10000
200
220
240
260
Wavelength (nm)
LYS
Released LYS

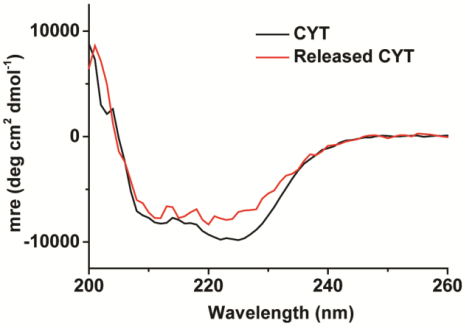
mre (deg cm^2 dmol^{-1})
10000
0
-10000
200
220
240
260
Wavelength (nm)
CYT
Released CYT

Figure 2.S2 *CD spectra of free proteins (black) and the released proteins from MSNs (or AEP-MSNs) (red) in PBS, pH 7.4, 25 °C. Concentration of non-encapsulated and encapsulated proteins were matched to provide accurate comparisons.*

Table 2.S1 Physical characteristics of MSNs and AEP-MSNs

Sample	BET surface area (m^2/g)	Channel volume (cm^3/g)	Channel diameter (nm)[a]
MSNs	506	1.01	10 ± 1
MSNs/CYT	263	0.56	7.5 ± 1.5
MSNs/Hb	275	0.58	7.5 ± 1.5
AEP-MSNs	318	0.71	9 ± 1
AEP-MSNs/LAC	203	0.42	6.5 ± 1.5
AEP-MSNs/CAT	223	0.46	6.5 ± 1.5

[a]*Calculated from the desorption branch of the N_2 sorption isotherms based on the BJH method.*

2.5 References

1. Z. Gu, A. Biswas, M. Zhao and Y. Tang, *Chem. Soc. Rev.*, **2011**, 40, 3638-3655.
2. B. Leader, Q. J. Baca and D. E. Golan, *Nat. Rev. Drug Discovery*, **2008**, 7, 21-39.
3. K. Epler, D. Padilla, G. Phillips, P. Crowder, R. Castillo, D. Wilkinson, B. Wilkinson, C. Burgard, R. Kalinich, J. Townson, B. Chackerian, C. Willman, D. Peabody, W. Wharton, C. J. Brinker, C. Ashley and E. Carnes, *Adv. Healthcare Mater.*, **2012**, 1, 348-353.
4. M. X. Zhao, B. L. Hu, Z. Gu, K. I. Joo, P. Wang and Y. Tang, *Nano Today*, **2013**, 8, 11-20.
5. D. Mahony, A. S. Cavallaro, F. Stahr, T. J. Mahony, S. Z. Qiao and N. Mitter, *Small*, **2013**, 9, 3138-3146.
6. D. D. Li, N. Kordalivand, M. F. Fransen, F. Ossendorp, K. Raemdonck, T. Vermonden, W. E. Hennink and C. F. van Nostrum, *Adv. Funct. Mater.*, **2015**, 25, 2993-3003.
7. F. P. Chang, Y. P. Chen and C. Y. Mou, *Small*, **2014**, 10, 4785-4795.
8. V. V. Shuvaev and V. R. Muzykantov, *J. Controlled Release*, **2011**, 153, 56-63.
9. M. Wang, J. A. Zuris, F. T. Meng, H. Rees, S. Sun, P. Deng, Y. Han, X. Gao, D. Pouli, Q. Wu, I. Georgakoudi, D. R. Liu and Q. B. Xu, *Proc. Natl. Acad. Sci. U. S. A.*, **2016**, 113, 2868-2873.
10. P. Ghosh, X. C. Yang, R. Arvizo, Z. J. Zhu, S. S. Agasti, Z. H. Mo and V. M. Rotello, *J. Am. Chem. Soc.*, **2010**, 132, 2642-2645.
11. T. Vermonden, R. Censi and W. E. Hennink, *Chem. Rev.*, **2012**, 112, 2853-2888.
12. D. Tarn, C. E. Ashley, M. Xue, E. C. Carnes, J. I. Zink and C. J. Brinker, *Acc. Chem. Res.*, **2013**, 46, 792-801.
13. C. Argyo, V. Weiss, C. Bräuchle and T. Bein, *Chem. Mater.*, **2014**, 26, 435-451.
14. C.-H. Lee, T.-S. Lin and C.-Y. Mou, *Nano Today*, **2009**, 4, 165-179.
15. P. Yang, S. Gai and J. Lin, *Chem. Soc. Rev.*, **2012**, 41, 3679-3698.
16. Y.-J. Han, G. D. Stucky and A. Butler, *J. Am. Chem. Soc.*, **1999**, 121, 9897-9898.
17. J. F. Diaz and K. J. Balkus, *J. Mol. Catal. B: Enzym.*, **1996**, 2, 115-126.
18. N. Z. Knezevic and J. O. Durand, *Chempluschem*, **2015**, 80, 26-36.
19. M. Ma, H. R. Chen, Y. Chen, K. Zhang, X. Wang, X. Z. Cui and J. L. Shi, *J. Mater. Chem.*, **2012**, 22, 5615-5621.
20. L. C. Sang, A. Vinu and M. O. Coppens, *Langmuir*, **2011**, 27, 13828-13837.
21. C. Xu, M. H. Yu, O. Noonan, J. Zhang, H. Song, H. W. Zhang, C. Lei, Y. T. Niu, X. D. Huang, Y. N. Yang and C. Z. Yu, *Small*, **2015**, 11, 5949-5955.
22. Y. P. Chen, C. T. Chen, Y. Hung, C. M. Chou, T. P. Liu, M. R. Liang, C. T. Chen and C. Y. Mou, *J. Am. Chem. Soc.*, **2013**, 135, 1516-1523.
23. K. T. Mody, A. Popat, D. Mahony, A. S. Cavallaro, C. Yu and N. Mitter, *Nanoscale*, **2013**, 5, 5167-5179.
24. Z. W. Cai, Z. M. Ye, X. W. Yang, Y. L. Chang, H. F. Wang, Y. F. Liu and A. N. Cao, *Nanoscale*, **2011**, 3, 1974-1976.
25. I. I. Slowing, J. L. Vivero-Escoto, C. W. Wu and V. S. Y. Lin, *Adv. Drug Delivery Rev.*, **2008**, 60, 1278-1288.
26. T. F. Martens, K. Remaut, J. Demeester, S. C. De Smedt and K. Braeckmans, *Nano Today*, **2014**, 9, 344-364.
27. K. Moller, J. Kobler and T. Bein, *Adv. Funct. Mater.*, **2007**, 17, 605-612.
28. Y. Han and J. Y. Ying, *Angew. Chem., Int. Ed.*, **2005**, 44, 288-292.
29. S. H. Wu, C. Y. Mou and H. P. Lin, *Chem. Soc. Rev.*, **2013**, 42, 3862-3875.
30. A. B. D. Nandiyanto, S.-G. Kim, F. Iskandar and K. Okuyama, *Microporous Mesoporous Mater.*, **2009**, 120, 447-453.
31. J. Sun, H. Zhang, R. Tian, D. Ma, X. Bao, D. S. Su and H. Zou, *Chem. Commun.*, **2006**, 1322-1324.
32. M. Hartmann, *Chem. Mater.*, **2005**, 17, 4577-4593.
33. A. Katiyar, L. Ji, P. G. Smirniotis and N. G. Pinto, *Microporous Mesoporous Mater.*, **2005**, 80, 311-320.
34. S. Hudson, J. Cooney and E. Magner, *Angew. Chem., Int. Ed.*, **2008**, 47, 8582-8594.
35. J. Fan, J. Lei, L. Wang, C. Yu, B. Tu and D. Zhao, *Chem. Commun.*, **2003**, 2140-2141.

36. N. Z. Knezevic and J. O. Durand, *Nanoscale*, **2015**, 7, 2199-2209.
37. H. S. Shin, Y. K. Hwang and S. Huh, *ACS Appl. Mater. Interfaces*, **2014**, 6, 1740-1746.
38. F. Lu, S. H. Wu, Y. Hung and C. Y. Mou, *Small*, **2009**, 5, 1408-1413.
39. J. L. Vivero-Escoto, Slowing, II, B. G. Trewyn and V. S. Lin, *Small*, **2010**, 6, 1952-1967.
40. D. Y. Zhao, J. L. Feng, Q. S. Huo, N. Melosh, G. H. Fredrickson, B. F. Chmelka and G. D. Stucky, *Science*, **1998**, 279, 548-552.
41. Y. Han, D. F. Li, L. Zhao, J. W. Song, X. Y. Yang, N. Li, Y. Di, C. J. Li, S. Wu, X. Z. Xu, X. J. Meng, K. F. Lin and F. S. Xiao, *Angew. Chem., Int. Ed.*, **2003**, 42, 3633-3637.
42. Q. Y. Yu, J. F. Hui, P. P. Wang, B. Xu, J. Zhuang and X. Wang, *Nanoscale*, **2012**, 4, 7114-7120.
43. S. B. Hartono, N. T. Phuoc, M. H. Yu, Z. F. Jia, M. J. Monteiro, S. H. Qiao and C. Z. Yu, *J. Mater. Chem. B*, **2014**, 2, 718-726.
44. H. Zhang, J. M. Sun, D. Ma, X. H. Bao, A. Klein-Hoffmann, G. Weinberg, D. S. Su and R. Schlogl, *J. Am. Chem. Soc.*, **2004**, 126, 7440-7441.
45. A. Vinu, V. Murugesan, O. Tangermann and M. Hartmann, *Chem. Mater.*, **2004**, 16, 3056-3065.
46. Y. Wang and F. Caruso, *Chem. Commun.*, **2004**, 1528-1529.
47. Y. Urabe, T. Shiomi, T. Itoh, A. Kawai, T. Tsunoda, F. Mizukami and K. Sakaguchi, *Chembiochem*, **2007**, 8, 668-674.
48. Y. J. Wang and F. Caruso, *Chem. Mater.*, **2005**, 17, 953-961.
49. Y. Zhang, Z. Zhi, T. Jiang, J. Zhang, Z. Wang and S. Wang, *J. Controlled Release*, **2010**, 145, 257-263.
50. C. E. Ashley, E. C. Carnes, G. K. Phillips, D. Padilla, P. N. Durfee, P. A. Brown, T. N. Hanna, J. Liu, B. Phillips, M. B. Carter, N. J. Carroll, X. Jiang, D. R. Dunphy, C. L. Willman, D. N. Petsev, D. G. Evans, A. N. Parikh, B. Chackerian, W. Wharton, D. S. Peabody and C. J. Brinker, *Nat. Mater.*, **2011**, 10, 389-397.
51. W. Gao, B. Y. Sha, W. Zou, X. Liang, X. Z. Meng, H. Xu, J. Tang, D. C. Wu, L. X. Xu and H. Zhang, *Biomaterials*, **2011**, 32, 9425-9433.
52. E. P. J. Barrett, L. E.; HALENDA, P., *J. Am. Chem. Soc.*, **1951**, 73, 373-380.
53. I. I. Slowing, B. G. Trewyn and V. S. Y. Lin, *J. Am. Chem. Soc.*, **2007**, 129, 8845-8849.
54. C. T. Kresge, M. E. Leonowicz, W. J. Roth, J. C. Vartuli and J. S. Beck, *Nature*, **1992**, 359, 710-712.
55. S. Areva, C. Boissiere, D. Grosso, T. Asakawa, C. Sanchez and M. Linden, *Chem. Commun.*, **2004**, 1630-1631.
56. J. R. Matos, M. Kruk, L. P. Mercuri, M. Jaroniec, L. Zhao, T. Kamiyama, O. Terasaki, T. J. Pinnavaia and Y. Liu, *J. Am. Chem. Soc.*, **2003**, 125, 821-829.
57. D. H. Pan, P. Yuan, L. Z. Zhao, N. A. Liu, L. Zhou, G. F. Wei, J. Zhang, Y. C. Ling, Y. Fan, B. Y. Wei, H. Y. Liu, C. Z. Yu and X. J. Bao, *Chem. Mater.*, **2009**, 21, 5413-5425.
58. T. Ito, L. Sun, M. A. Bevan and R. M. Crooks, *Langmuir*, **2004**, 20, 6940-6945.
59. R. Schmidt, E. W. Hansen, M. Stocker, D. Akporiaye and O. H. Ellestad, *J. Am. Chem. Soc.*, **1995**, 117, 4049-4056.
60. L. Duan, X. H. Yan, A. H. Wang, Y. Jia and J. B. Li, *ACS Nano*, **2012**, 6, 6897-6904.
61. J. Mendez, M. Morales Cruz, Y. Delgado, C. M. Figueroa, E. A. Orellano, M. Morales, A. Monteagudo and K. Griebenow, *Mol. Pharmaceutics*, **2014**, 11, 102-111.
62. M. Hamborg, F. Rose, L. Jorgensen, K. Bjorklund, H. B. Pedersen, D. Christensen and C. Foged, *Biochim. Biophys. Acta*, **2014**, 1838, 2001-2010.
63. F. Meder, C. Brandes, L. Treccani and K. Rezwan, *Acta Biomater*, **2013**, 9, 5780-5787.
64. J. Ambati, A. M. Lopez, D. Cochran, P. Wattamwar, K. Bean, T. D. Dziubla and S. E. Rankin, *Acta Biomater.*, **2012**, 8, 2096-2103.
65. J. Wu, X. Li, Y. Yan, Y. Hu, Y. Zhang and Y. Tang, *J. Colloid Interface Sci.*, **2013**, 406, 130-138.
66. S. B. Hartono, S. Z. Qiao, K. Jack, B. P. Ladewig, Z. P. Hao and G. Q. Lu, *Langmuir*, **2009**, 25, 6413-6424.
67. R. Ravindra, Z. Shuang, H. Gies and R. Winter, *J. Am. Chem. Soc.*, **2004**, 126, 12224-12225.
68. E. Chiavazzo, M. Fasano, P. Asinari and P. Decuzzi, *Nat. Commun.*, **2014**, 5.